Temperature dependence of Mo-Au Gibbsian segregating alloys

Huatan Qiu
S. N. Srivastava
Keith C. Thompson
Martin J. Neumann
David N. Ruzic
University of Illinois at Urbana-Champaign
Center for Plasma Material Interactions
104 S. Wright Street
Urbana, Illinois 61801
E-mail: druzic@uiuc.edu

Abstract. A critical challenge for the success of extreme ultraviolet (EUV) lithography is to prevent collector mirror surface damage and reflectivity loss. Plasma debris and radiation damage the mirror and degrade the reflectivity. We study an innovative approach to the design and fabrication of collector mirror surface materials to improve collector lifetime. A Mo-Au Gibbsian segregation (GS) alloy is developed on silicon using a dc dual-magnetron cosputtering system, and the temperature effect on mirror damage is investigated. Result shows that a thin Au segregating layer is maintained during exposure, even though overall erosion is taking place. The reflective material underneath the segregating layer, Mo, is protected by the Au sacrificial layer, which is preferentially sputtered. Both theoretical and experimental studies have been performed to prove the effectiveness of the GS alloys for use as an EUV collector optics material.
[DOI: 10.1117/1.2964218]

Subject terms: EUV lithography; Gibbsian alloys; collector mirror.

Paper 07087R received Oct. 27, 2007; revised manuscript received Apr. 14, 2008; accepted for publication May 5, 2008; published online Aug. 11, 2008.

1 Introduction

To meet the advancing expectations of Moore's law, next-generation lithography (NGL) methods are needed. Current light sources can extend the current lithography light regime down to 45 nm and even 32 nm nodes through various resolution enhancement techniques; however, beyond that EUV sources producing light[1–5] at 13.5 nm are the leading NGL candidates.

Much research is focused on developing an extreme ultraviolet (EUV) source; however, there are certain challenges to be resolved in order to successfully implement this technology for high-volume manufacturing (HVM) applications. Two types of plasma sources, the discharge-produced plasma and the laser-produced plasma are being studied as potential EUV sources. Xenon (Xe) and tin (Sn) are used as the fuel materials for these sources to produce EUV at extremely high charge states on the order of +10. Both of the source types also produce strong electric fields during plasma expansion that can accelerate ions to high energies on the order of 10 keV. The high flux of energetic ions will bombard the collector optics, damaging the surface and diminishing the reflectivity of the mirror.

Mirror degradation is caused by surface erosion, roughening, deposition, implantation of impurities, and layer mixing. To test the performance of various EUV mirror materials during operation of a commercial-scale EUV source and to investigate the mechanisms behind any observed losses in reflectivity, the Xtreme Commercial EUV Emission Device (XCEED) at the University of Illinois[6,7] has been developed. Debris mitigation schemes[8,9] are also being developed extensively to reduce the ion fluxes and energies to prevent the mirror surface from being damaged. The advancements in these areas are still too limited to support the HVM environment. Another way of increasing the collector optics lifetime is to engineer damage-resistant or self-healing mirrors. If these mirrors could be developed to maintain good surface smoothness and high reflectivity over a longer period of time, it would advance the EUV lithography (EUVL) development process and reduce the cost of ownership due to repair and replacement of optics assemblies.

The innovative idea of using the Gibbsian segregation (GS) concept in the design of grazing incidence EUV collector optics is developed and explored.[10,11] The GS process has been defined as the tendency of certain solute elements in a homogenously interspersed solid solution to accumulate at imperfections, such as grain boundaries and interfaces in the bulk lattice, which then may segregate to the free surfaces.[12] Because GS processes and phenomena occur at the surface, there is the potential for functional surface engineering to achieve the desired physical, chemical, electrical, and optical effects. The energy deposition from EUV and out-of-band light, together with the bombardment by energetic ion debris, provides the potential driving force for GS processes to occur at the surface. For example, in a Mo-Au GS alloy, the segregation of Au (solute) will replenish the mirror surface from the bulk material of the GS alloy so that the surface-segregating Au serves as a sacrificial sputtering layer and leaves the Mo underneath virtually untouched. If the regenerative transport processes (bulk, grain, interface diffusions) and surface renormalization are faster than the erosion time scale (i.e., the average time between large energy sputtering events), then the collector optics will be self-repairing. Work has been done to assess the suitability of the GS alloy technology for early adoption in EUVL and to test its validity with theoretical estimates.[10,11] The present work describes further experi-

1537-1646/2008/$25.00 © 2008 SPIE

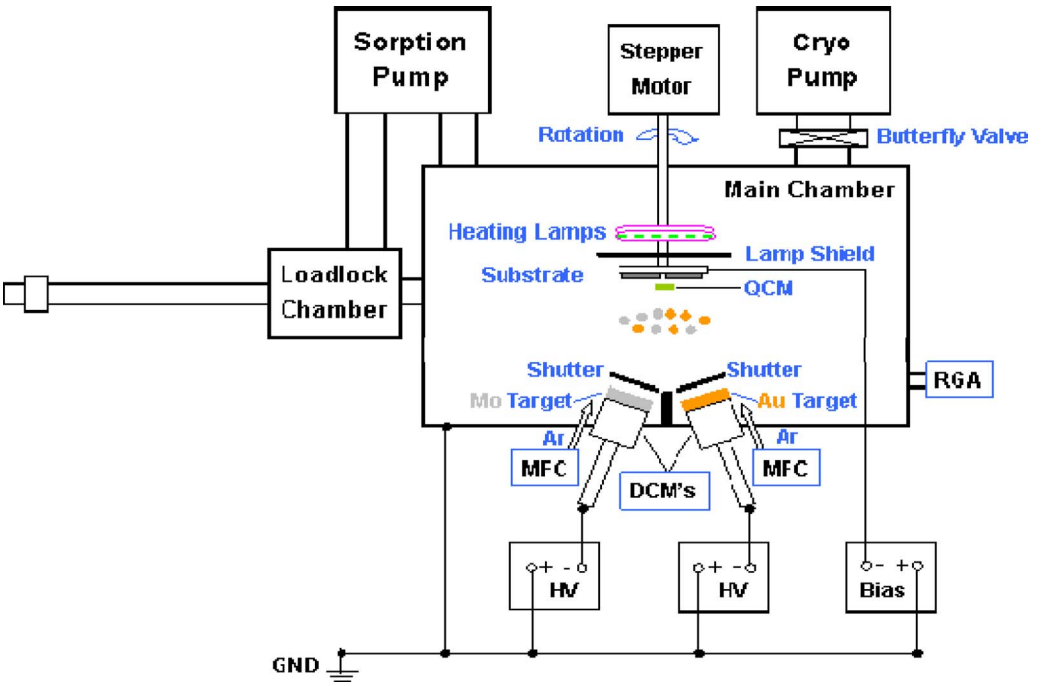

Fig. 1 The DMCS operating with two dc magnetron guns.

mental efforts to determine if GS alloys effectively ameliorate and self-heal the damage in grazing incidence EUV collector optics. In particular, the effect of temperature on the mirror surface erosion, surface composition, and surface roughness is studied. *In situ* reflectivity measurements are also performed to investigate the temperature effect on the GS performance.

2 Experiment

High quality Mo-Au GS alloys are fabricated using a dual-magnetron cosputtering system (DMCS) at Illinois. The Mo-Au GS samples are exposed in a Xe-fueled EUV source, and the resulting erosion, surface composition, and roughness is measured using scanning electron microscopy (SEM), auger electron spectroscopy (AES), and atomic force microscopy (AFM). In addition, the *in situ* reflectivity is measured from these samples as they are exposed.

2.1 *DMCS Fabrication System*

The Mo-Au GS alloys are produced in the DMCS system at the Center for Plasma Material Interactions (Fig. 1), which is capable of making layered thin-film depositions or alloying two materials together on a heated substrate. Several features of the DMCS system are designed to produce the high-quality Mo-Au GS films. The base pressure of the deposition chamber is able to be maintained at an ultrahigh vacuum of $\sim 4 \times 10^{-9}$ Torr to keep a clean and oxygen-free environment for the deposition process. The substrate, with samples mounted, is designed to allow for heating and biasing, and can be rotated. All possible sources of oxygen or air are minimized throughout the whole process. The experimental parameters (e.g., temperature and sample bias) are carefully determined based on stringent quality requirements. Because there are two targets (Mo at 99.95% purity and Au at 99.99% purity) in use simultaneously, the sputtered atoms will prefer to diffuse toward the substrate in a certain solid angle with respect to their own target location. Therefore, it is necessary to continuously rotate the substrate so that both Mo and Au contents will reach the sample surfaces uniformly. This is achieved using a rotary motion feedthrough with a programmable stepper motor. Additionally, ultrahigh purity (UHP) Ar is used as operation gas and controlled using mass flow controllers. The Mo and Au sputtering targets are precleaned at high power levels by sputtering for at least 15 min with the shutters closed to remove the surface oxide and contamination layer prior to sample fabrication. To inhibit the formation of the native surface oxide layer, a capping layer of ~3 nm Au is created to protect the film from oxidation in all runs and to provide a higher initial surface enrichment of Au.[13–15] In actual use as a collector mirror, this capping layer would be quickly eroded to a thickness on the order of a few atomic layers (~0.5 nm), thus activating the segregation process. The Mo-Au GS alloys are fabricated with a recipe of 165°C, 2 mTorr UHP Ar, −100-V dc bias, 65-W dc power on the Mo target and 1.7-W dc power on the Au target. The alloy ratio of Au is controlled in the range of 1–2% to avoid a significant reflectivity loss to the EUV light. The root-mean-square (rms) surface roughness is maintained at 1 nm or less to fit the requirement dictated for mirror films in EUV collector optics.

2.2 *Sample Exposure System*

An XTREME XTS 13-35 DPP EUV source is mated with an XCEED diagnostics setup, shown in Fig. 2. This apparatus allows mirror samples to be exposed to the *z*-pinch Xe plasma for a specified number of pinches, then removed and examined to determine the damage. The XCEED exposure tool is also designed to allow for the characterization of the EUV source plasma and the debris fields emitted

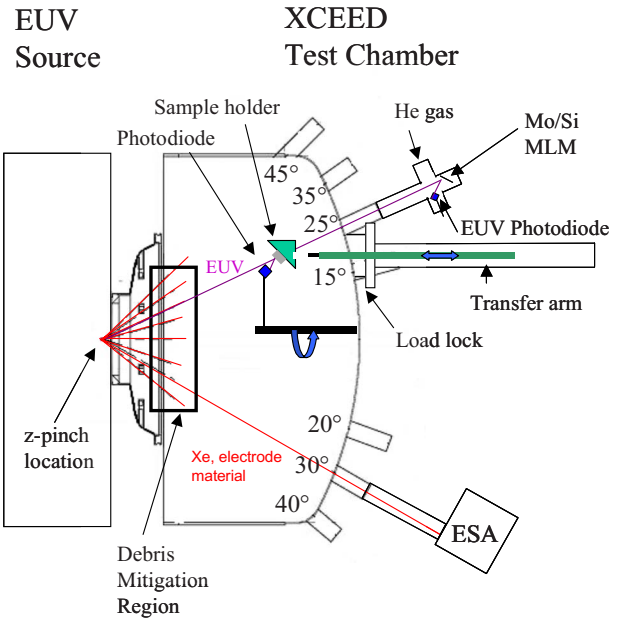

Fig. 2 The schematic diagram of the XCEED exposure tool.

Fig. 4 The typical oscilloscope signals of the *in situ* reflectivity measurement. The top line indicates the reflection signal. The middle line indicates the pinch signal (IGBT). The bottom line indicates the reference signal.

by it. The energy sector analyzer (ESA)[6,7] is used to measure ion debris emitted from the plasma source, selecting particles by energy-to-charge ratio and using ion time-of-flight analysis to identify the species. There are four sample locations in the XCEED chamber. Each has a mounting port, load lock extraction port, viewing window, and thermocouple feed-through for temperature measurement. The samples can be preheated by the halogen lamp array before exposure and measured by the thermocouple sensors attached on the sample holders. However, the lamps and the thermocouple sensors cannot work once the plasma pinch starts, possibly because of strong ion-flux bombardments from the pinch plasma during operation. Therefore, only preheating is achieved instead of continuous *in situ* heating, which might lessen the thermal performance of GS. A load-lock system is used to remove one sample at a time, without disturbing the conditions seen at the other sample locations.

This is critical to minimize transient effects that are caused by electrode thermal cycling from discontinuous source operation. The sample holders are custom-designed aluminum blocks with indentations for mirror sample positioning. Samples are attached with carbon tape to the sample holders and positioned to present the samples to the light source at either a ~20 deg grazing or ~70 deg normal incidence angle. In the present experiment, all samples are investigated at the grazing incidence.

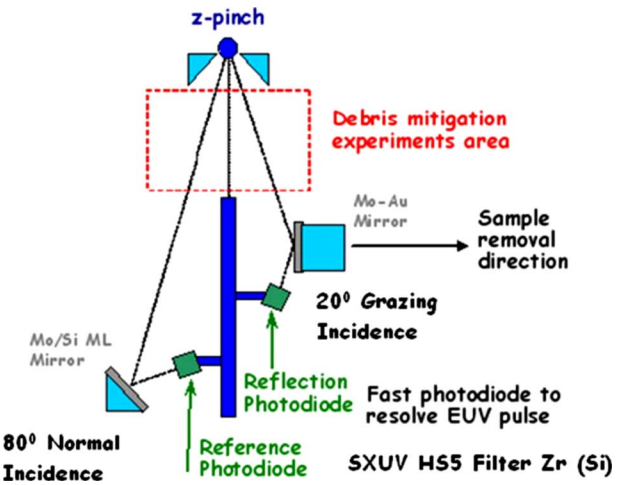

Fig. 3 The schematic diagram of the *in situ* reflectivity measurement in XCEED system.

2.3 *In situ Reflectivity Measurement*

The mirror samples are placed at a distance of 56 cm from the pinch at ~20 deg grazing incidence angle. EUV light from the source is measured directly ("reference"), and also after being reflected by the samples ("reflection"). This is done using two international radiation detectors[16] SXUV HS5 Zr/Si EUV photodiodes. Wavelength selectivity is provided by a built-in Zr/Si filter, limiting the amount of out-of-band radiation that contributes to the signal. The *in situ* reflectivity measurement configuration is shown in Fig. 3. The reference photodiode (88.7 cm from pinch) is mounted external to the chamber on an angled port in a single-bounce configuration. EUV light is reflected from a specialized Mo/Si multilayer mirror that provides further in-band selectivity for EUV light measurements. The 50-bilayer mirror is placed in the path of the reference EUV light at 10-deg-to-normal incidence, reflecting the light toward the reference photodiode 4.2 cm away. This is done to protect the reference photodiode against the direct bombardment of energetic ion debris during the measurements. Additionally, there is a 2-mm orifice limiting particle flux, and the assembly is backfilled with helium gas to mitigate damage to the multilayer mirror. The EUV light reflected by the mirror samples mounted in the chamber is detected by another photodiode placed 3.2 cm away from the leading edge of the sample. This photodiode is contained in an aluminum shield to protect it from debris damage and to prevent stray light from adding to the measured signal. It is

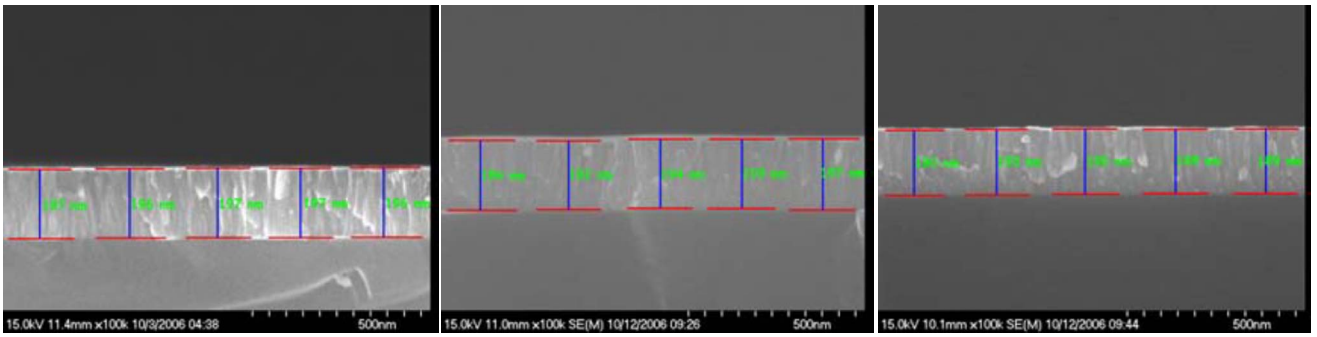

Fig. 5 The cross-sectional pictures of the pre- and postexposed Mo-Au samples: (a) Preexposed Mo-Au sample with a ~3-nm Au capping layer, (b) postexposed Mo-Au sample with a preheat temperature of 187°C, and (c) postexposed Mo-Au sample with a preheat temperature of 102°C.

affixed to the shaft of a Kurt J. Lesker Company Model No. KZRD275037HS motorized rotary feed-through and can be rotated to measure reflected EUV light from any of the four sample locations in the chamber.

The EUV selectivity of the photodiodes is governed by the reflectivity of the mirror combined with the responsivity of the filtered photodiode. The resulting bandwidth is ~4%. Typically, the response of the photodiode to the EUV light emitted during a single pinch is a narrow positive peak, as shown in Fig. 4. Integrating the pulse area provides a value for the total energy of EUV light emitted in units of volt-seconds. This can be directly converted to a value in traditional units if the reflectivity of the single bounce mirror and the characteristic response of the photodiode are accurately known. Ideally, the plasma source would maintain a consistent level of EUV output independent of exposure time. This is not guaranteed, however; thus, the reference photodiode is used to provide an independent measurement of the source's EUV output level over time. The *in situ* photodiode measurement is then compared to the reference measurement to provide a value for the reflectivity of the sample mirrors. Finally, each of the relative reflectivity measurements will be normalized to their maximum, in order to eliminate the impacts of the variation of the measure angle, the instability of the plasma pinch size, and the other operational variations between different sample locations and different exposures. Moreover, the individual *in situ* reflectivity measurements can be qualitatively compared to each other in this normalized scale.

3 Results and Discussion

Two GS Mo-1.08%(±0.16%)Au samples, referred to as "Post 1" and "Post 2," are exposed to 3.32 million shots in a Xe-fueled EUV source. Both samples are preheated to investigate the effect of temperature on the sample surface. Both the samples (Post 1 and Post 2) are raised initially to a temperature of 184 and 102°C, respectively. The final temperatures of the two samples are, similarly, 66 and 61°C. The *in situ* reflectivity measurements are performed using two EUV photodiodes at 20 deg grazing incidence angle. Because GS diffusion is exponentially sensitive to the temperature, it is expected that the performance of the GS sample at high temperature will be better than the one at low temperature, with respect to GS diffusion, surface self-healing, erosion resistance, and maintained reflectivity. In theory, a higher temperature will cause stronger GS diffusion so that the Au might diffuse onto the surface at a faster rate than it would in the sample at a lower temperature.

Erosion on the samples due to energetic plasma debris is measured with SEM and is displayed in Fig. 5. The results are summarized in Table 1. As can be seen, the SEM-measured erosion of the Mo-Au sample with a higher preheat temperature and the one with a lower preheat temperature are 2.1 and 6.9 nm, respectively. The two exposed Mo-Au samples show different degrees of erosion due to the different GS performance under different temperature. We believe the sample at higher temperature shows less erosion as a result of thermally enhanced GS effect on the erosion resistance.

Sample erosion is also theoretically calculated and compared to the experimental measurement. Ion debris in the existing Xe EUV source is measured with the ESA at 200 cm from the pinch, operating at 100 Hz without any buffer gas. More detail on the ion debris measurement can be found in earlier publications.[6,7,17]

Using the measured ion fluxes with the ESA and the calculated sputtering yields using "The Stopping and Range of Ions in Matter" (SRIM) code,[18] the removal rate of the Au capping layer and the erosion rate in bulk Mo-1% Au or pure Mo from different ion species are calculated. Prediction of the removal rate of segregating material from the surface during exposure can be approximated simply by

Table 1 SEM results of the Mo-Au samples of the temperature exposure experiment (error = 1 nm).

Sample	Thickness (nm)	Erosion (nm)	Note
Preexposed	196.6	–	–
Post 1	194.5	2.1	High preheat temp.
Post 2	189.7	6.9	Low preheat temp.

Table 2 Number density of different layer structure of Mo-Au GS alloy.

Material	Structure Constant, (Å)	Atomic Weight W_t, (g/mol)	Physical Density ρ, (g/cm^3)	Number Density (number per cm^2 layer)
Mo	3.147	95.940	10.28	2.03×10^{15}
Au	4.0782	196.967	19.30	2.41×10^{15}

summarizing the amount of segregated material removed from the surface by all energetic ion fluxes with their different energies (corresponding to different sputtering yields). This can be mathematically described as follows:

$$R_{\text{removal}}(t) = \gamma(t) f \sum_{i,j} \Gamma_{i,j}(t) Y_{i,j} + \cdots, \tag{1}$$

where f is the exposure frequency of the ion pulse; i refers to the ion species; j indicates the incident energy of ion species i; $\Gamma_{i,j}(t)$ is the relative ion flux per pulse of species i with energy j, reaching on the surface. Y_{ij} is the sputtering yield of Au due to the bombardment of species i with energy j. Sputtering yield is determined using the SRIM code. $\gamma(t)$ is the atomic concentration (in atomic percent) ratio of the segregating material (Au) in the surface segregating layer. Ideally, $\gamma=1$ for a thin 100%-segregated Au layer. For a pure Mo film, $\gamma=0$ without segregation. Note that there are more terms that could be added to the removal rate in Equation (1) to account for deposition, implantation, and reflection. These are second-order effects and are ignored in this work.

The ESA is fully calibrated to measure the ion debris

Table 3 Theoretical erosion calculations of temperature exposure experiment. This is a sample table showing the erosion calculation only for Xe^+ ions.

Xe^+ Energy Spectra		Au Capping Layer		Mo-1%Au with Ideal Segregating		Pure Mo	
Ion Energy (keV)	56 cm Flux Rate (#/cm^2 s)	Sputter Yield: Au of Mo-Au	Removal Flux Rate (#/cm^2 s)	Sputter Yield: Mo of Mo-Au	Erosion Rate (nm/min)	Sputter Yield: Pure Mo	Erosion Rate (nm/min)
1	1.1×10^{9}	4.4	4.8×10^{9}	0.009	8.83×10^{-8}	3.0	3.1×10^{-5}
2	2.2×10^{9}	7.3	1.6×10^{10}	0.048	9.61×10^{-7}	5.2	1.0×10^{-4}
3	4.2×10^{9}	9.8	4.1×10^{10}	0.107	4.14×10^{-6}	6.9	2.7×10^{-4}
4	9.5×10^{9}	11.8	1.1×10^{11}	0.174	1.54×10^{-5}	8.4	7.5×10^{-4}
5	2.6×10^{10}	13.7	3.6×10^{11}	0.248	5.98×10^{-5}	9.7	2.3×10^{-3}
6	4.2×10^{10}	15.5	6.5×10^{11}	0.323	1.27×10^{-4}	10.8	4.3×10^{-3}
7	5.6×10^{10}	16.9	9.5×10^{11}	0.394	2.04×10^{-4}	11.9	6.2×10^{-3}
8	6.9×10^{10}	18.5	1.3×10^{12}	0.468	3.01×10^{-4}	12.9	8.3×10^{-3}
9	5.6×10^{10}	19.7	1.1×10^{12}	0.536	2.78×10^{-4}	13.8	7.1×10^{-3}
10	4.2×10^{10}	21.1	8.9×10^{11}	0.614	2.42×10^{-4}	14.6	5.7×10^{-3}
11	2.6×10^{10}	22.3	5.8×10^{11}	0.684	1.65×10^{-4}	15.4	3.7×10^{-3}
12	9.5×10^{9}	23.4	2.2×10^{11}	0.746	6.62×10^{-5}	16.1	1.4×10^{-3}
13	4.2×10^{9}	24.6	1.0×10^{11}	0.814	3.15×10^{-5}	16.8	6.5×10^{-4}
14	2.2×10^{9}	25.6	5.5×10^{10}	0.881	1.77×10^{-5}	17.4	3.5×10^{-4}
15	1.1×10^{9}	26.6	2.9×10^{10}	0.943	9.69×10^{-6}	18.0	1.8×10^{-4}
Total Au Removal Flux		6.4×10^{12}					
Erosion Rate (nm/min)		6.5×10^{-2}		1.5×10^{-3}		4.1×10^{-2}	

Table 4 Predicted erosion rates due to each ion species identified in the *z*-pinch source.

20-deg Grazing, 100 Hz	Erosion Rate (nm/min)		
Ion Species	Au Capping Layer	Mo-1%Au w/Ideal Segregating Layer	Pure Mo
Xe^{+}	6.5×10^{-2}	1.5×10^{-3}	4.1×10^{-2}
Xe^{+2}	2.4×10^{-1}	6.1×10^{-3}	1.5×10^{-1}
W^{+}	4.0×10^{-3}	4.8×10^{-5}	2.6×10^{-3}
Mo^{+}	9.3×10^{-4}	2.0×10^{-5}	5.8×10^{-4}

Table 5 Summary of the theoretical prediction of the erosion rate, erosion time and total erosion for Au, Mo-1%Au and pure Mo.

20-deg Grazing	Au Capping Layer	Mo-1%Au with Ideal Segregating Layer	Pure Mo
Pinch Frequency (Hz)	100	100	100
Total Erosion Rate (nm/min)	0.308	0.008	0.196
Erosion Time (min)	10	120	120
Erosion (nm)	3	0.9	23.5
Total Erosion (nm)		0.9	25.5

and energy spectra in absolute units [number of ions/cm^2-pulse-eV]. Previous work showed good agreement between measured fluxes and observed erosion rates using this same method.[17] The measured ion energy spectrum at a distance of 200 cm from the pinch is divided into energy bins with a bin size of $\Delta E=1$ keV, and the corresponding area under the curve is calculated, in order to get the integrated ion flux in these bins. Subsequently, the flux rate can be calculated as $f\Delta E\Sigma\Gamma_{i,j}$ in absolute units [number of ions per cm^2/s], after careful calibration at the actual sample location (56 cm from the pinch—multiplying by a factor assuming a simply r^2 geometric dependence). The conversion ratio in the present work is $(200\ \text{cm}/56\ \text{cm})^2=12.76$. In order to predict erosion, the measured ion energy data is fed into SRIM code to run in a Monte Carlo simulation. The sputtering yields of the film materials by the ion species incident at 20 deg grazing angle at different energies are then calculated. The removal rates of the individual ion species can be obtained after multiplying by the corresponding sputtering yields. The sum of the individual removal rates gives the total removal rate of the film materials (Au or Mo), in the units of [number of removed atoms/cm^2 s].

Using the removal rate of Eq. (1), the erosion can be predicted using

$$\Delta T_{\text{erosion}}=\int\frac{dt}{\rho_{\text{alloy}}A_v}\sum_k R^k_{\text{removal}}(t)W^k_t, \tag{2}$$

where ρ_{alloy} is the physical density [g/cm^3] of the segregating layer of Mo-Au alloy; k=Mo or Au, indicates the eroded component of the alloy; A_v is Avogadro's number [number mole]; $R^k_{\text{removal}}(t)$ and W^k_t are the removal rate [Eq. (1)] and atomic weight [grams/mole] of component k, respectively.

The number density of each layer of the Mo-Au GS alloy is also needed to predict the erosion and calculated using

$$\frac{\text{No. density}}{\text{layer}}=A_v\left(\frac{\rho a}{W_t}\right)_{\text{majority}}\left(\frac{\#}{\text{cm}^2-\text{layer}}\right). \tag{3}$$

The number densities of the Au capping layer and the Mo bulk layer are 2.41×10^{15} and 2.03×10^{15} per cm^2 layer, respectively. The data are summarized in Table 2. The erosion rates at the different layers can be predicted based on the obtained number density of each layer. In theory, the sum of the contributions of all ions from the pinch plasma gives the total erosion rate at each layer.

In the experiment, the erosive ion species mainly include xenon (fuel gas), tungsten and molybdenum (materials from the vicinity of the electrodes), and argon if buffer gas applied. The corresponding ion energy ranges from 1 to 16 keV for the dominating xenon ions, and 1 to 8 keV for other minor ion species. The film materials include pure Ru, pure Mo, and Mo-1%Au GS alloy. To evaluate the erosion resistance of the Mo-Au GS alloy, two extreme configurations are chosen. One is the pure Mo film without Au ($\gamma=0$), indicating the zero GS efficiency. The other is Mo-1%Au film with an ideal 0.5-nm segregating Au layer on the surface ($\gamma=1$), indicating an ideal GS alloy with maximum efficiency. In the ideal case, bulk Au will continuously segregate onto the top surface and maintain at the thickness of a few monolayers (assume $d=0.5$ nm). The GS has the maximum efficiency in erosion resistance in the ideal situation, and the minimum efficiency in the pure Mo case. The ~3 nm Au capping layer could be removed within the first tens of minutes. Then the erosion rate in bulk Mo entirely depends on the segregation performance. If the segregating layer of Au could be well maintained due to the effectively regenerative transport and surface renormalization, then the erosion of Mo could be greatly prevented.

Table 3 summarizes the theoretical erosion calculations caused by only Xe^+ ions. Using the ESA, Xe^{2+}, W^+, and Mo^+ are also identified as coming from the pinch plasma thus, similar calculations are performed to calculate the erosion from these components. Table 3 only presents a sample table considering the single-species xenon ions. Finally, the total erosion rates from all ion species are calculated and shown in Table 4. The contributions from Xe^+ and

Table 6 Comparisons of erosion between theoretical prediction and experimental measurements in temperature exposure experiment.

Erosion comparison [calculation and measurement]		
	High Temp.	Low Temp.
Preheated Temperature (°C)	187	102
Ideal Mo-1%Au (nm)	0.9	
Pure Mo (nm)	25.5	
SEM Measurement (nm)	2.1±1	6.9±1
Theoretical GS Efficiency (%)	95	76

Xe^{+2} are still dominant in total erosive flux, ~98.4, 99.1, and 98.3% of the total erosion in the Au-capping layer, ideal Mo-1%Au bulk, and pure Mo bulk, respectively. Therefore, a ~3-nm-Au-capping layer would be removed after ~10 min of 100 Hz exposure (~0.2 million shots), approximating the actual removal time of the Au capping layer measured to be ~10 to15 min (as determined by reflectivity measurements shown later). Table 5 summarizes the theoretical erosion prediction. Theoretically, the total erosion rates at 100 Hz operation are 0.308 nm/min for the Au capping layer, 0.008 nm/min for the Mo-1%Au bulk and 0.196 nm/min for the pure Mo bulk. The theoretical predictions in erosion have been compared to the experimental measurements by SEM in Table 6. As seen in this table, the theoretical GS efficiencies of the high- and low-temperature samples are 95 and 76%, respectively. A rise of 85°C in the preheated temperature results in an increase of 19.4% in GS efficiency with respect to erosion resistance to a removal flux rate of 3.03×10^{13} cm^2 s.

AES is performed to investigate the surface composition. Figures 6(a)–6(c) show that the Mo-Au sample with higher temperature has ~12% surface Au atomic percent, whereas the one with lower temperature has ~5% surface Au atomic percent after 3.32 million EUV exposure shots. This result shows evidence of Gibbsian segregation. The atomic percent of Au on the surface after up to ~6.9 nm erosions is still much higher (~5–12%) than the bulk Au atomic percent (~1.08%), which proves that the GS does work to segregate bulk Au onto the surface even when the surface Au is eroded. The difference in surface Au atomic percent implies that the higher preheated temperature helps to activate a stronger GS diffusion in the same exposure scale as the lower preheated temperature, so that a larger Au atomic percent can been seen on the surface of the exposed Mo-Au sample. The lower preheated Mo-Au GS sample (at 102°C) seems to be less efficient in segregating bulk Au onto the eroded surface by the GS process, leading to a larger erosion (6.9 nm) and lower final atomic percent of surface Au (~5%).

AFM is performed to investigate the surface roughness

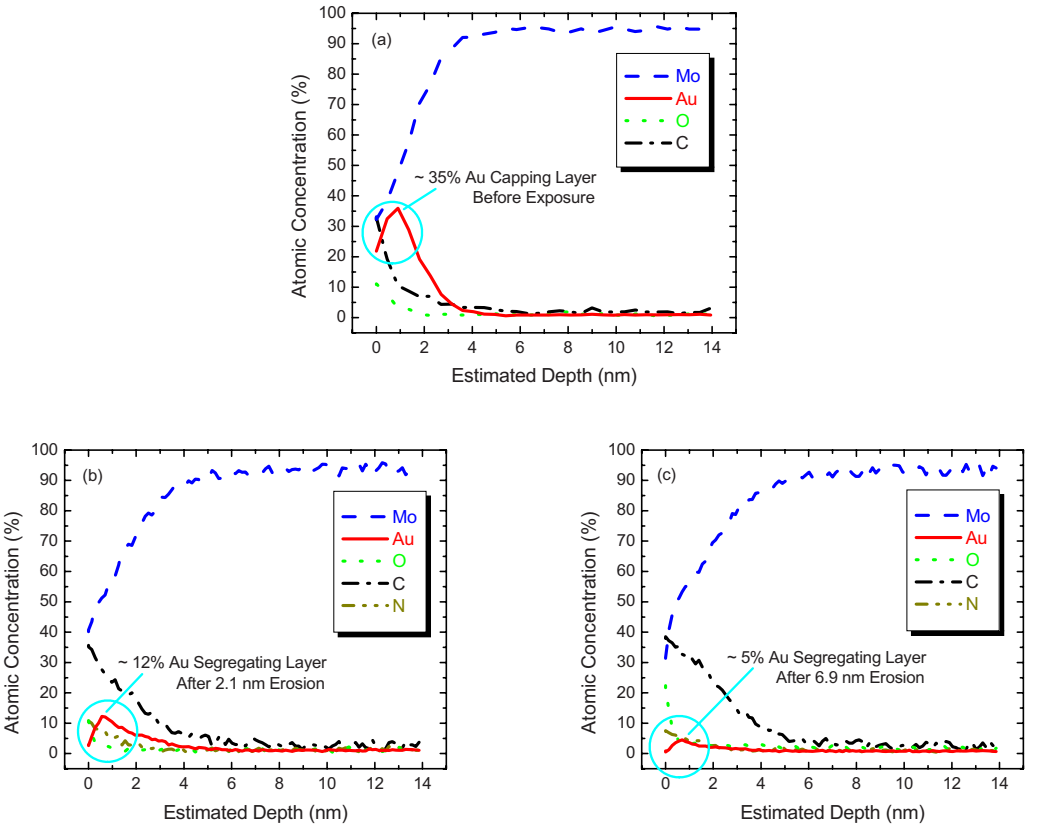

Fig. 6 The depth profiles of the pre- and postexposed Mo-Au samples: (a) Preexposed Mo-Au sample with a ~3-nm Au capping layer, (b) postexposed Mo-Au sample with a preheat temperature of 187°C, and (c) postexposed Mo-Au sample with a preheat temperature of 102°C.

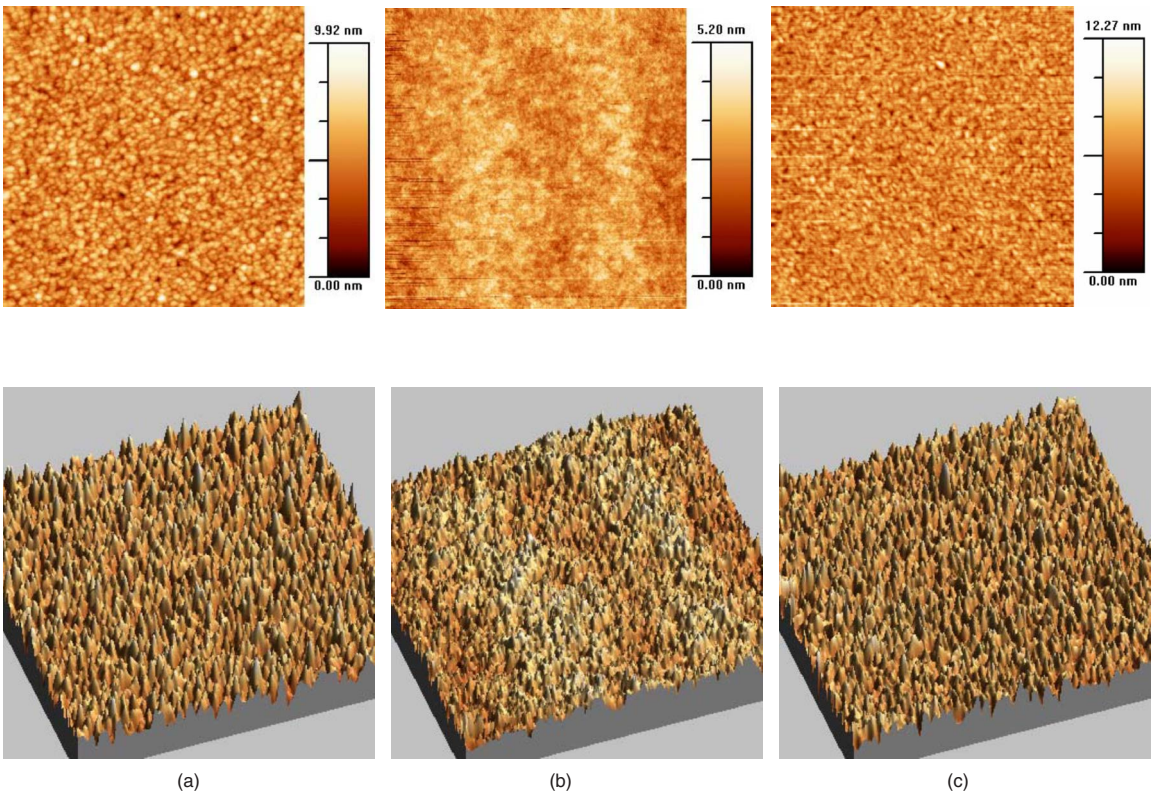

Fig. 7 The rms roughness of the pre- and postexposed Mo-Au samples in 2-D and 3-D modes: (a) Preexposed Mo-Au sample with a ~3-nm Au capping layer, (b) postexposed Mo-Au sample with a preheat temperature of 187°C, and (c) postexposed Mo-Au sample with a preheat temperature of 102°C.

and compared for the different temperature samples. Figures 7(a)–7(c) show the Mo-Au samples after 3.32 million EUV shot exposure and it is observed that it does not become significantly rougher as compared to the preexposed sample. Moreover, the Post 1 Mo-Au sample with a higher preheat temperature actually becomes smoother by 0.49x at 0.54 nm rms roughness, while the other sample, Post 2, slightly increased in roughness by 1.12x at 1.23 nm rms roughness as listed in Table 7. The overall heights of the columnar islands (indicated by H_{max}) of the pre- and post-Mo-Au samples are also coincident with the rms roughness results due to the sufficient and insufficient GS performances, respectively. Again, this implies that the GS effect of self-healing does work to repair the eroded surface during the exposure, and the higher preheat temperature helps to enhance this self-healing effect by activating a stronger GS diffusion to efficiently induce more Au segregating onto the roughened surface.

Table 7 AFM results of the Mo-Au samples for temperature exposure experiment. The rms roughness and maximum height is measured for all the samples.

Sample	rms Roughness (nm)	Change (Posf/Pre)	Maximum Height (nm)	Note
Preexposed	1.10	–	10.68	–
Post 1	0.54	0.49x	6.61	High Preheat Temp.
Post 2	1.23	1.12x	12.63	Low Preheat Temp.

In situ reflectivity is measured on the exposed samples at 56 cm from the pinch at 20 deg grazing (70 deg to the nor-

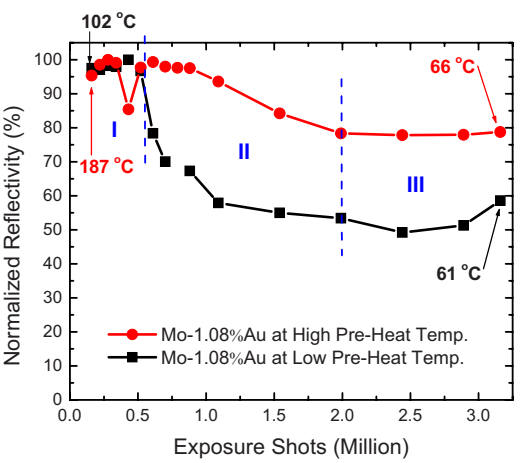

Fig. 8 The normalized reflectivity measurements of the Mo-1.08%Au samples exposed for 3.32 million Xe EUV shots. Top curve indicates the postexposed Mo-Au sample with a higher preheat temperature of 187°C. Bottom curve indicates the postexposed Mo-Au sample with a lower preheat temperature of 102°C.

Table 8 Summary of the results for the exposed Mo-Au samples for temperature exposure experiment.

Preheat Result	High Temp.	Low Temp.	Higher Temp. Helps GS to
Surface Au (at. %)	~12	~5	Promote bulk Au segregating onto the surface.
Roughness Change	0.49x	1.12x	Lessen the surface roughness by self-healing.
Maximum Height (nm)	6.61	12.63	Lessen the columnar islands by self-healing.
Erosion (nm)	2.1±1	6.9±1	Resist the erosion in Mo bulk.
Theoretical Efficiency (%)	95.2	75.8	
Degradation Start Time (M)	0.79	0.43	Postpone the start of the reflectivity degradation.
Equilibrium Reflectivity (%)	78.2	54.2	Maintain the reflectivity at higher equilibrium level.

mal) incidence angle. To explain the GS behavior, a simple three-period model is proposed.

1. Period I: In this region, the Au capping layer is almost removed and GS process is just initiated.
2. Period II: In this region, the GS process is fully activated and promoted to self-heal the eroded surface toward the new equilibrium between GS and erosion.
3. Period III: In this region, the GS process reached its new equilibrium to dynamically balance the steady erosion to maintain the reflectivity at a new equilibrium level.

Finally, the normalized reflectivity is calculated and shown in Fig. 8. As shown, the change in the normalized reflectivity of the exposed Mo-Au sample meets with the definitions of the three characteristic GS periods. In GS period I, the reflectivity increases a little bit because the thin Au capping layer (~3 nm) is removed by ion debris until a few monolayers left. Then, in GS period II, the reflectivity degradation takes place because of the further erosion in Mo. In this region, the GS is fully activated to work against the reflectivity degradation by segregating more Au onto the surface. Finally, in GS period III, the reflectivity is kept relatively flat again but at a lower level when a new equilibrium between GS and erosion is achieved. The time scale (exposure scale) for the reflectivity degradation and the new equilibrium reflectivity differ under the different temperature, removal rate, and other experimental conditions of the exposed Mo-Au samples. According to the results seen in Fig. 8, the reflectivity degradation starts after 0.79 million shots and 0.43 million shots for the exposed Mo-Au samples with higher and lower preheated temperatures, respectively. The new equilibrium levels are, similarly, 78.2 and 54.2% with respect to their maxima. This shows the obvious enhancement to the GS performance that the higher preheated temperature provides for postponing the reflectivity degradation and maintaining a new equilibrium at a higher level. It is also evidence for GS, because the reflectivity does not continuously drop down to an unacceptably low level, especially under such a high removal flux. The segregating Au from bulk of the Mo-Au alloy does work to effectively diffuse onto the surface, self-heal the eroded surface, resist the erosion of the reflective Mo material, and reduce the reflectivity degradation. Table 8 summarizes the results for the exposed Mo-Au samples for temperature exposure experiments.

4 Conclusions

This paper studies an innovative approach on design and fabrication of collector mirror surface material for longevity of collector lifetime. The temperature effects are investigated on Mo-1%Au samples for the effectiveness of GS in order to maintain the self-regenerative and erosion-resisting surface. Postexposed material characterization and *in situ* reflectivity measurement shows that the GS performance at a higher preheated temperature helps to prevent surface damage and reflectivity degradation. The further improvement on the GS efficiency is believed to be achievable if the *in situ* heating is available to maintain the GS mirror at the elevating temperature. The comparison to the pure Mo mirror, however not in terms of the temperature effect, is investigated in the other works.[19]

Acknowledgments

We are thankful for the support from SEMATECH, Lawrence Livermore National Laboratory, Sandia National Laboratory at Livermore, Intel Components Research, and Xtreme Technologies GmbH. We also thank Prof. Angus Rockett for providing the original deposition equipment. A portion of this research was carried out in the Center for Microanalysis of Materials, University of Illinois, which is partially supported by the U.S. Department of Energy under

Grant No. DEFG02-91-ER45439. We also thank our undergraduate Jesse C. Anderson for the help with GS alloy fabrication and the buildup of DMCS system.

References

1. H. Kinoshita, "History of extreme ultraviolet lithography," *J. Vac. Sci. Technol. B* **23**, 2584–2588 (2005).
2. U. Stamm, "Extreme ultraviolet light sources for use in semiconductor lithography: state of the art and future development," *J. Phys. D* **37**, 3244 (2004).
3. Y. Teramoto et al., "Development of Xe- and Sn-fueled high-power Z-pinch EUV source aiming at HVM," *Proc. SPIE* **6151**, 615147 (2006).
4. D. C. Brandt et al., "LPP EUV source development for HVM," *Proc. SPIE* **6517**, 65170Q (2007).
5. M. Corthout et al., "Sn DPP source modules: status of alpha resources, beta developments, and the scalability to HVM," *Proc. SPIE* **6921**, 69210V (2008).
6. Keith C. Thompson, E. L. Antonsen, M. R. Hendricks, B. E. Jurczyk, M. Williams, and D. N. Ruzic, "Experimental test chamber design for optics exposure testing and debris characterization of a xenon discharge produced plasma source for extreme ultraviolet lithography," *Microelectron. Eng.* **83**, 476 (2006).
7. E. L. Antonsen, K. C. Thompson, M. R. Hendricks, D. A. Alman, B. E. Jurczyk, and D. N. Ruzic, "Ion debris characterization from z-pinch extreme ultraviolet light source," *J. Appl. Phys.* **99**, 063301 (2006).
8. D. N. Ruzic, "Origin of Debris in EUV Sources and its Mitigation," Chapter 36 in *EUV Sources for Lithography*, Vivek Bakshi, Ed., SPIE Press, Bellingham, WA (2006).
9. D. N. Ruzic, K. C. Thompson, B. E. Jurczyk, E. L. Antonsen, S. N. Srivastava, and J. B. Spencer, "Reduction of ion energies from multicomponent Z-pinch plasma," *IEEE Trans. Plasma Sci.* **35-3**, (2007).
10. H. Qiu, K. C. Thompson, S. N. Srivastava, E. L. Antonsen, D. A. Alman, B. E. Jurczyk, and D. N. Ruzic, "Optical exposure characterization and comparisons for discharge produced plasma Sn extreme ultraviolet system," *J. Micro/Nanolith. MEMS MOEMS* **5**, 033007 (2006).
11. D. A. Alman, H. Qiu, T. Spila, K. C. Thompson, E. L. Antonsen, B. E. Jurczyk, and D. N. Ruzic, "Characterization of collector optic material samples exposed to a discharge-produced plasma extreme ultraviolet light source," *J. Micro/Nanolith. MEMS MOEMS* **6**, 013006 (2007).
12. P. A. Dowben and A. Miller, *Surface Segregation Phenomena*, CRC Press, Boca Raton (1990).
13. S. Bajt et al., "Design and performance of capping layers for extreme-ultraviolet multilayer mirrors," *Appl. Opt.* **42**, 5750 (2003).
14. L. Gan, R. D. Gomez, C. J. Powell, R. D. Mcmichael, P. J. Chen, and W. F. Egelhoff, Jr, "Thin Al, Au, Cu, Ni, Fe, and Ta films as oxidation barriers for Co in air," *J. Appl. Phys.* **93**, 8731 (2003).
15. S. Bajt, Z. R. Dai, E. J. Nelson, M. A. Wall, J. B. Alameda, N. Q. Nguyen, S. L. Baker, J. C. Robinson, and J. S. Taylor, "Oxidation resistance and microstructure of ruthenium-capped extreme ultraviolet lithography multilayers," *J. Microlithogr., Microfabr., Microsyst.* **5**, 023004 (2006).
16. Intemational Radiation Detectors Inc., Torrance, CA, ⟨www.ird-inc.com⟩
17. S. N. Srivastava, K. C. Thompson, E. L. Antonsen, H. Qiu, J. B. Spencer, D. Papke, and N. Ruzic, "Lifetime measurements on collector optics from Xe and Sn extreme ultraviolet sources," *J. Appl. Phys.* **102**, 023301 (2007).
18. J. F. Ziegler, *The Stopping and Range of Ions in Solids*, Pergamon, New York (1985).
19. H. Qiu, S. N. Srivastava, K. C. Thompson, M. J. Neumann, and D. N. Ruzic, "The effectiveness of Mo-Au Gibbsian segregating (GS) alloys and the surface removal effect on the GS performance for EUV collector optics," *Opt. Eng.* (submitted).

Biographies and photographs of the authors not available.